IEEE Access
Multidisciplinary | Rapid Review | Open Access Journal

Date of publication xxxx 00, 0000, date of current version xxxx 00, 0000.

Digital Object Identifier 10.1109/ACCESS.2019.Doi Number

Gas source declaration with tetrahedral sensing geometries and median value filtering extreme learning machine

Hui-Rang Hou[1], Achim Lilienthal[2] and Qing-Hao Meng[1] (Member, IEEE)

[1]The authors are with Tianjin Key Laboratory of Process Measurement and Control, Institute of Robotics and Autonomous Systems, School of Electrical and Information Engineering, Tianjin University, Tianjin, China.
[2]Mobile Robotics and Olfaction Lab, AASS, School of Science and Technology, Örebro University, Sweden.

Corresponding author: Q. H. Meng (e-mail: qh_meng@tju.edu.cn).

This work was supported by the National Natural Science Foundation of China (No. 61573253), and National Key R&D Program of China under Grant (No. 2017YFC0306200).

ABSTRACT Gas source localization (including gas source declaration) is critical for environmental monitoring, pollution control and chemical safety. In this paper we approach the gas source declaration problem by constructing a tetrahedron, each vertex of which consists of a gas sensor and a three-dimensional (3D) anemometer. With this setup, the space sampled around a gas source can be divided into two categories, i.e. inside ("source in") and outside ("source out") the tetrahedron, posing gas source declaration as a classification problem. For the declaration of the "source in" or "source out" cases, we propose to directly take raw gas concentration and wind measurement data as features, and apply a median value filtering based extreme learning machine (M-ELM) method. Our experimental results show the efficacy of the proposed method, yielding accuracies of 93.2% and 100% for gas source declaration in the regular and irregular tetrahedron experiments, respectively. These results are better than that of the ELM-MFC (mass flux criterion) and other variants of ELM algorithms.

INDEX TERMS Gas source declaration, tetrahedron, gas concentration measurement, wind information, extreme learning machine, median value filtering.

I. INTRODUCTION

Localization (including declaration) of hazardous or flammable gas leakages is of great significance in environmental monitoring, security of large factory warehouses, investigation of fire sources, inspection of prohibited items such as drugs, and search and rescue of disaster survivors [1]-[5].

Gas sources can be localized using manually collected gas measurements [6]. However, for reasons of personnel safety, locating (including declaring) the gas source by search teams is in many cases not a viable solution [7]. Accordingly, a quickly deployable, unmanned measurement device is needed. Researchers started to study robots for gas source localization (including declaration) in the early 1990s [8]–[11]. At present, much source localization (including declaration) research based on two-dimensional (2D) platforms, e.g., gas sensor networks [12]–[27] and 2D robot active olfaction (RAO) [28]–[40], have achieved good results. Given that gas diffusion is actually three-dimensional (3D), it is important to study 3D gas source localization (including declaration) [41]–[44]. Ishida et al. [45] developed a robotic system based on a blimp to track a gas/odor plume three-dimensionally and to search for its source. The large balloon of the blimp was employed as part of a gas sensing system by placing an array of gas sensors distributed over the balloon surface. The sensors facing toward the gas source exhibit "active" responses whereas the sensors behind the large balloon body show "quiet" responses. However, blimps have an unfavorable size-to-payload ratio and are heavily affected by wind. Rather than a blimp, an unmanned aerial vehicle (UAV) was adopted by Kuroki et al. [46]. An expert system for contaminant mapping based on a genetic algorithm was presented [46]. This method was tested by simulations using a Gaussian plume/puff model. Neumann et al. [47, 48] used a gas sensitive microdrone to obtain a gas distribution map and localize gas sources. Luo et al. [49] designed a flying odor compass that can be used for gas plume tracking (a step of gas source localization). The compass was built on a quadrotor helicopter and contains three gas

sensors. Considering the practical application, this paper focuses on gas source declaration in 3D environment.

To declare a gas source efficiently, it is essential to collect wind measurements [50]. In fact, wind vector estimation, including wind speed and direction, is very important as it can provide valuable information for estimating the direction towards the gas source. In a 2D environment, in general, accurate wind information can be obtained by using anemometers [51, 52]. However, the weight of anemometers reduces the available payload and the flight time of the flying robots drastically [49]. That is, due to the limited payloads, anemometers are not applicable for flying robots such as UAVs, microdrones and quadrotor helicopters. For this reason some authors have proposed to estimate wind information without anemometers. Neumann et al. [47] proposed a method to derive an estimate of air flow without a dedicated anemometer. That was using the UAV controller to compensate for air flow. To track the gas source precisely in a windy environment, Wei et al. [6] arranged three gas sensors in a regular triangle. Based on this sensor placement method, a scale-space method used for obtaining the feature information of multi-time scale, a feature-point matching algorithm to calculate time series of the sensor data and a graphical statistical method to estimate the direction of the gas source were presented. Luo et al. [49] combined the continuous wavelet with modulus maxima algorithm to estimate the direction which the gas comes from.

In summary, for gas source declaration, it is important and necessary to study the 3D gas source declaration problem, and it is useful to obtain accurate gas concentration and wind information. Regarding the declaration of 3D gas sources, many types of flying robots have been adopted or designed. However, when these flying robots are used in practice, they face a number of difficulties such as the large disturbance of the rapidly rotating rotors to the surrounding airflow, the limited accuracy of wind estimation and their short endurance. The airflow will be affected by the flying robots, especially the gas flow field near the flying robots will be seriously disturbed, which affects the judgement of gas concentration and impedes flying robots for real-time applications. Further, the wind information obtained by the estimation algorithms is far less accurate than that measured by an anemometer, and the robustness of alternative wind estimation methods is not clearly described in the literature. Last but not the least, flying robots require sufficient power, while it is difficult to provide long-term battery life. Therefore, an alternative gas source declaration strategy that can be used in 3D environments is required.

In this paper, the aforementioned limitations of flying robots are taken into consideration and a 3D gas source declaration approach is proposed using a tetrahedral sensor structure without using a flying robot. Each tetrahedral vertex is composed of a gas sensor and a 3D anemometer. From sequences of measurements with this tetrahedral sensor structure we aim to distinguish two cases corresponding to the situation where a gas source is inside the tetrahedron ("source in") or not ("source out"). In order to use all available information, including the gas concentration and wind information, we propose to use the raw measured gas concentration and wind data to classify "source in" against "source out" cases. For this classification, we present in this paper a median value filtering based extreme learning machine (M-ELM) method. The remainder of this paper is organized as follows. Section II describes the tetrahedral arrangement of sensor nodes. Section III introduces the hardware setup. Section IV details the M-ELM based gas source declaration method. In Section V, the experimental results are presented. Section VI concludes the paper, and Section VII looks ahead to future works.

II. TETRAHEDRON MODEL

A. TETRAHEDRON-BASED GAS SOURCE DECLARATION

The purpose of gas source declaration is to determine whether a gas source is in the immediate vicinity [29] or determine the certainty that the source has been found [33, 34]. By constructing a tetrahedron of sensor nodes (see Figs. 1 and 2 (b)), which can be irregular, the gas source declaration problem can be converted to a two-class classification whether the gas source is inside ("source in" case) or outside ("source out" case) the tetrahedron. The reason we choose the tetrahedron is that it requires the least number of gas sensors and anemometers among all the 3D structures, which is the most economical and practical approach.

B. TWO WAYS FOR TETRAHEDRON CONSTRUCTING

Constructing a tetrahedron from four sensor nodes is the hardware basis for the proposed gas source declaration method. Here, two theoretical ways for tetrahedron construction are presented. One is based on a fixed sensor node structure (each sensor node consists of a gas sensor and a 3D anemometer), and another one is based on a mobile sensor node structure.

1) Fixed sensor node structure

Tetrahedral sensor node structures using fixed sensor nodes are shown in Fig. 1. Each tetrahedron works independently, so multiple gas sources can be detected simultaneously by the designed multi-tetrahedral structure.

2) Mobile Sensor Node Structure

To reduce the number of sensor nodes and reduce installation and calibration issues in a space with obstacles, a structure with mobile sensor nodes was designed, which needs only four sensor nodes. Its schematic diagram is shown in Fig. 2.

The hardware of our tetrahedral sensing structure is composed of several sensor nodes represented by black balls, moved along square grid guide rails installed on the roof with pulleys and ropes. Each pulley is installed in a movement device (as shown in Fig 2(b)) and connected to

This article has been accepted for publication in a future issue of this journal, but has not been fully edited. Content may change prior to final publication. Citation information: DOI 10.1109/ACCESS.2019.2963059, IEEE Access

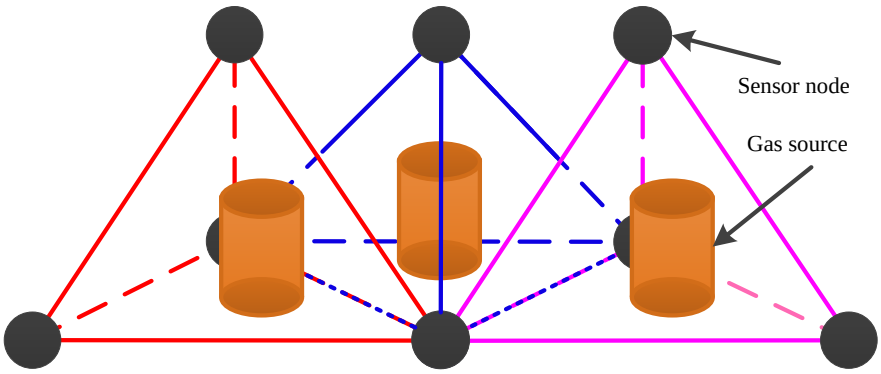

FIGURE 1. **Tetrahedral constructions with fixed sensor node structure.**

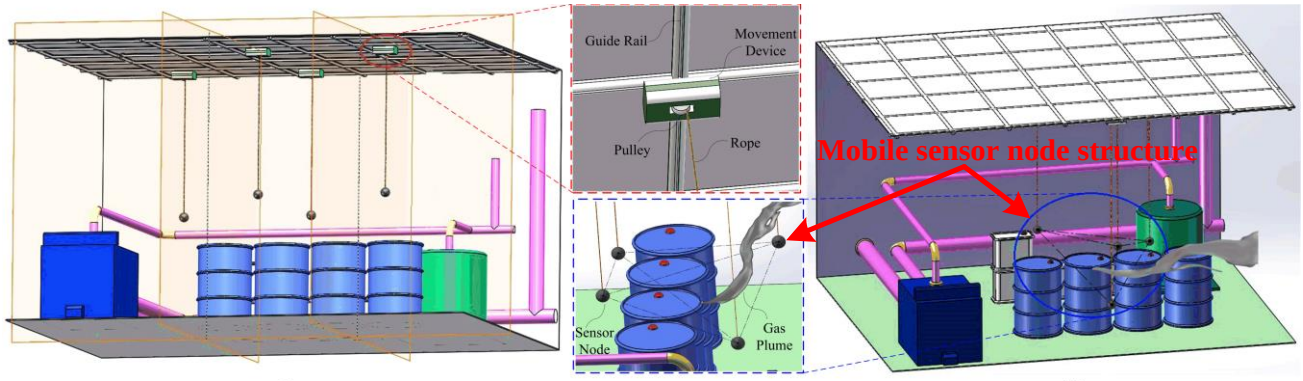

(a) Gas detection stage (b) Tetrahedral construction stage

FIGURE 2. **Tetrahedral constructions with a mobile sensor node structure. (a) and (b) represent the gas detection stage and the tetrahedral construction stage, respectively.**

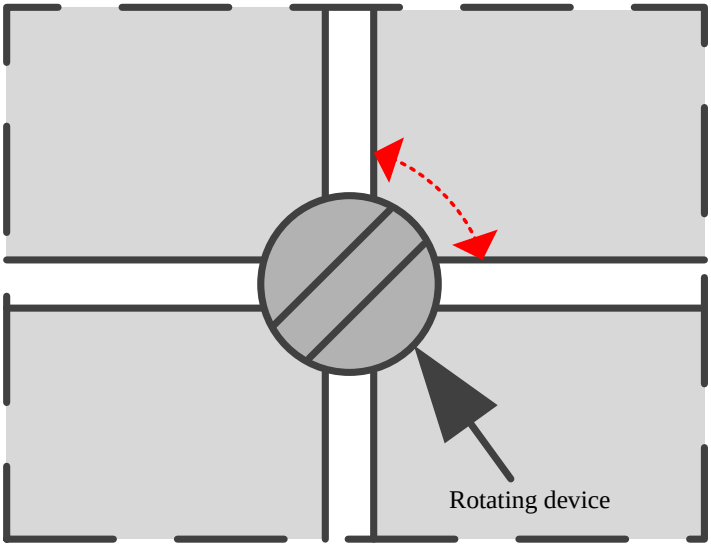

FIGURE 3. **Through rotation of a movement device, its direction on the rails can be changed.**

one end of a rope. The other end of the rope is connected to a sensor node composed of a gas sensor and a 3D wind anemometer. The height of a sensor node can be controlled through driving the pulley by the corresponding movement device. As shown in Fig. 3, there is also a rotating device that can be rotated within 360 degrees at every grid

This article has been accepted for publication in a future issue of this journal, but has not been fully edited. Content may change prior to final publication. Citation information: DOI 10.1109/ACCESS.2019.2963059, IEEE Access

intersection. In this way, the movement device can change its direction.

With the device shown in Fig. 3, 3D movements of the sensor nodes can be realized. In real-world applications, to effectively construct a tetrahedron, an obstacle map and a feasible 3D path planning strategy including 2D path planning and height adjustment of the sensor nodes are needed. The proposed 3D path planning strategy is illustrated in the Supporting Information.

III. EXPERIMENTAL SETUP

In the current research stage, the tetrahedron-based gas source declaration method was experimentally verified, and a 3D path planning strategy (as shown in the Supporting Information) is verified by simulation. Our experimental setup is shown in Fig. 4. Four modules, each consisting of a wireless gas sensor and a 3D anemometer, were used as vertices to construct a tetrahedral structure. The gas sensor model used was a MiCS-5521, and among four anemometers, three of them were a Young 81000 model and the fourth was a Gill R3-50 model.

The gas sensors and the anemometers were used to collect alcohol volatile, i.e., gas concentrations and wind vectors, respectively. The gas sensors were calibrated in a container which was filled with ethanol vapor of a controlled concentration. Before the experiment, the baseline voltage V_{base} of each gas sensor was measured in clean air. The gas response voltage V_{res} indicating the measured gas concentration was then calculated as $V_{res} = V_{sen} - V_{base}$, where V_{sen} represents the detected sensor voltage. As gas source we used a cup containing pure ethanol, which was heated to accelerate the evaporation process. The gas concentration data was measured with a frequency of 20 Hz, and the anemometer data was down-sampled to 20 Hz because of the anemometers' higher output rates. For each tetrahedral vertex, four values, i.e., a gas sensor response voltage and three wind speed values along the x, y, and z directions can be obtained at the same time. In this way, for the four tetrahedral vertices, 16 values can be obtained at the same time, which we use directly as 16 feature values of one sample.

IV. M-ELM RECOGNITION ALGORITHM

The tetrahedron-based gas source declaration procedure is illustrated in Fig. 5. The proposed gas source declaration methods are described in detail in this section.

As a classic learning framework, extreme learning machine (ELM) has been extended to different research fields and gained great progresses. An incremental ELM (I-ELM) was proposed in the following [53], where the hidden nodes were randomly generated and the output weights were analytically calculated. In the case of online sequential learning, an online sequential extreme learning algorithm (OS-ELM) was developed [54, 55]. With the OS-ELM, data can be learned one-by-one or chunk-by-chunk with fixed or varying chunk size and the input data can be processed sequentially. Huang et al. [56] extended ELM for both semisupervised and unsupervised tasks based on the manifold regularization, and the unlabeled or partially labeled samples are clustered using ELM. To obtain satisfactory feature learning performance, in which the original ELM and/or the aforementioned variants may not achieve, a multilayer learning architecture using ELM-based autoencoder as basic building block, was developed in the following [57]. The original inputs were decomposed into multiple hidden layers, and the outputs of the previous layer were used as the inputs of the current one. Recently, to improve on the I-ELM, bidirectional extreme learning machines (B-ELMs) were developed in the following [58]. The B-ELM separates the odd and even learning steps. At the

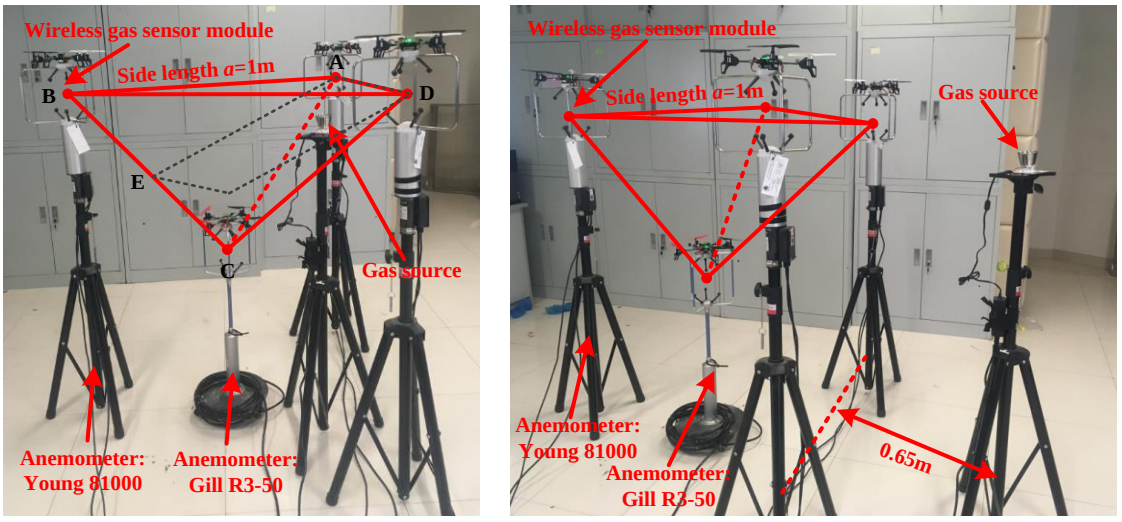

(a) "source in" case (b) "source out" case

FIGURE 4. Positional relation between the tetrahedron and the gas source. The gas sensors were attached to a quadrotor helicopter and the quadrotor helicopter was placed on top of an anemometer. The panels show the case where a gas source is inside (a) or outside (b) the tetrahedron.

odd learning step, a hidden node was added like I-ELM. At the even learning step, a new hidden node was added via a formula based on the formerly added node results. However, some of the hidden nodes generated by the I-ELM may play a minor role; thus, the increase in network complexity due to the B-ELM may be unnecessary. To avoid this issue, an enhanced B-ELM method (referred to as EB-ELM) was proposed in the following [59]. Several hidden nodes were randomly generated at each odd learning step, however, only the nodes with the largest residual error reduction would be added to the existing network.

The main characteristic of ELM and the above improved algorithms is that the network weights are random [60]. When such algorithms are used for classification, the results are also somewhat random. To reduce the randomness of the results, we propose to use 50 ELM algorithms at the same time and find the median average value of the 50 ELM output results, termed median value filtering based extreme learning machine (M-ELM).

In this study, the raw measurements at one instance in time, including four gas sensor response voltages and twelve wind speed values, are fed into the median value filtering based extreme learning machine (M-ELM) classifying the sixteen features as "source in" or "source out".

Figure 6 shows the principle of the M-ELM algorithm, which is a simple neural network algorithm containing three layers, namely, input layer, hidden layer and output layer. A detailed explanation of the M-ELM follows.

(1) Input layer: $\mathbf{x}$ is the feature vector which is taken as the inputs of the M-ELM algorithm.

$$\mathbf{x}=[\mathbf{x}_1 \quad \cdots \quad \mathbf{x}_d]^T_{d\times n} \tag{1}$$

d is the total number of samples for training or testing. $\mathbf{x}_i$ is the feature vector of the ith sample, and n (n=16 in this paper) is the feature dimension.

(2) Hidden layer: The hidden layer contains a number of L neurons (L=20 in this paper) and is fully connected to the input layer, see Eq. (2).

$$\mathbf{G}=\begin{bmatrix} g(\mathbf{w}_1.\mathbf{x}_1+\mathbf{b}_1) & \cdots & g(\mathbf{w}_L.\mathbf{x}_1+\mathbf{b}_L) \\ \cdots & \cdots & \cdots \\ g(\mathbf{w}_1.\mathbf{x}_d+\mathbf{b}_1) & \cdots & g(\mathbf{w}_L.\mathbf{x}_d+\mathbf{b}_L) \end{bmatrix}. \tag{2}$$

As shown in Fig. 6, $\mathbf{w}_i$ and $\mathbf{b}_i$ are the input weight and threshold of the ith neuron of the hidden layer, respectively. The activation function $g(\cdot)$ is a sigmoid function.

(3) Output layer: The output layer is fully connected to the hidden layer, see Eq. (3),

$$\mathbf{G}\boldsymbol{\beta}=\mathbf{S}, \tag{3}$$

where

$$\boldsymbol{\beta}=\begin{bmatrix} \boldsymbol{\beta}_1^T \\ \cdots \\ \boldsymbol{\beta}_L^T \end{bmatrix}_{L\times m}, \tag{4}$$

$$\mathbf{S}=\begin{bmatrix} \mathbf{S}_1^T \\ \cdots \\ \mathbf{S}_L^T \end{bmatrix}_{d\times m}. \tag{5}$$

m=2 is the class number, $\boldsymbol{\beta}$ is the transformation matrix between the hidden layer and the output layer, and $\mathbf{S}$ is an transition matrix of the target recognition results.

When the M-ELM algorithm is used for training, $\mathbf{S}$ is determined by the training samples:

$$\mathbf{S}_{jl}=\begin{cases} 1 & \text{correct class label} \\ 0 & \text{wrong class label} \end{cases}, \; l=1, 2, \ldots, m. \tag{6}$$

$\mathbf{S}_{jl}$ is the class label of the lth position of the jth training sample in the matrix $\mathbf{S}$.

When the M-ELM algorithm is used for testing, $\mathbf{S}$ is a matrix to be solved. For each sample, two values of $\mathbf{S}_{j1}$ and $\mathbf{S}_{j2}$ corresponding to the "source in" and "source out" are obtained in one recognition process. According to [60], the recognition accuracy tended to be stable when the number of ELM classifiers [63]-[65] was larger than 50. Considering the computational complexity and the stability, 50 ELM recognitions were performed in the M-ELM method, and then 50 $\mathbf{S}_{j1}$ and $\mathbf{S}_{j2}$ combinations (recorded as $\mathbf{S}_{j1}^1, \mathbf{S}_{j1}^2, \ldots, \mathbf{S}_{j1}^{50}$ and $\mathbf{S}_{j2}^1, \mathbf{S}_{j2}^2, \ldots, \mathbf{S}_{j2}^{50}$) corresponding to 50 ELMs can be obtained.

Taking the jth testing sample as an example, writing for simplicity, $\mathbf{S}_{j1}^1, \mathbf{S}_{j1}^2, \ldots, \mathbf{S}_{j1}^{50}$ and $\mathbf{S}_{j2}^1, \mathbf{S}_{j2}^2, \ldots, \mathbf{S}_{j2}^{50}$ are re-expressed as vectors $\mathbf{o}^1=[\mathbf{o}_1^1, \mathbf{o}_2^1, \ldots, \mathbf{o}_{50}^1]^T$ and $\mathbf{o}^2=[\mathbf{o}_1^2, \mathbf{o}_2^2, \ldots, \mathbf{o}_{50}^2]^T$, respectively. The calculation process of the recognition result vector $\mathbf{c}$ is described in Eqs. (7-10).

$$\mathbf{P}=\begin{bmatrix} \mathbf{p}_1^1, \mathbf{p}_2^1, \ldots, \mathbf{p}_{50}^1 \\ \mathbf{p}_1^2, \mathbf{p}_2^2, \ldots, \mathbf{p}_{50}^2 \end{bmatrix}=\begin{bmatrix} \text{sort}(\mathbf{o}_1^1, \mathbf{o}_2^1, \ldots, \mathbf{o}_{50}^1) \\ \text{sort}(\mathbf{o}_1^2, \mathbf{o}_2^2, \ldots, \mathbf{o}_{50}^2) \end{bmatrix}, \tag{7}$$

where the function sort(·) sorts all values from small to large. The sort values corresponding to "source in" and "source out" classes are stored in vectors $\mathbf{p}_1^1, \mathbf{p}_2^1, \ldots, \mathbf{p}_{50}^1$ and $\mathbf{p}_1^2, \mathbf{p}_2^2, \ldots, \mathbf{p}_{50}^2$, respectively. The effect of median value filtering in the M-ELM algorithm is to filter out the smallest and largest values in an array or a vector, and then average the remaining values. Here, we filter out the smallest 5 values and the largest 5 values, and the remaining values are averaged.

$$\begin{bmatrix} \mathbf{o}_1 \\ \mathbf{o}_2 \end{bmatrix}=\begin{bmatrix} \text{ave}(\mathbf{p}_6^1, \mathbf{p}_7^1, \ldots, \mathbf{p}_{45}^1) \\ \text{ave}(\mathbf{p}_6^2, \mathbf{p}_7^2, \ldots, \mathbf{p}_{45}^2) \end{bmatrix}. \tag{8}$$

The function ave(·) in Eq. (8) calculates the average value of the vector. Finally we decide whether the sample belongs to the class "source in" or "source out" using Eq. (9):

$$\mathbf{c}_j=\text{argmax}(\mathbf{o}_1, \mathbf{o}_2), \tag{9}$$

The function argmax(·) returns the position (or label) corresponding to the maximum in a vector, and the recognition result of the jth testing sample is recorded as $\mathbf{c}_j$. For the d testing samples, the recognition results are finally stored in a vector $\mathbf{c}$.

$$\mathbf{c}=\left[\mathbf{c}_j\right]. \tag{10}$$

V. EXPERIMENT VALIDATION

In this section, we examine the performance of the proposed method for gas source declaration.

A. Experiment and Data Descriptions

Regular tetrahedron experiments with different side lengths were first carried out in an indoor natural ventilation environment. Side lengths of the three regular tetrahedrons were set to 1.0 m, 1.5 m and 2.0 m. In each regular tetrahedron experiment, 2000 training samples (1000 "source in" and 1000 "source out") and 2000 testing samples (1000 "source in" and 1000 "source out") were obtained by using an MFC-based sample filter [62].

Further, an irregular tetrahedron experiment was carried out to verify that the proposed recognition algorithm can also work adequately for irregular tetrahedrons. Based on the regular tetrahedron with a side length of 1 m (Fig. 4), two of the four tetrahedral vertices were moved: one was raised by 0.1 m and the other one was lowered by 0.1 m to construct an irregular tetrahedron. For the irregular tetrahedron experiment, also 2000 training samples (1000 "source in" and 1000 "source out") and 2000 testing samples (1000 "source in", 1000 "source out") were collected. For each sample, the raw gas concentration measurements (represented by gas sensor response voltages) and 3D wind data were used as features for recognition.

B. Recognition Accuracy of Regular Tetrahedron

For gas source declaration, it was shown that using the mass flux features, the ELM-MFC (mass flux criterion) method can obtain a good recognition performance [62]. In this paper, we use a 16-dimensional feature vector composed of the gas sensor response voltages and the 3D wind speed measurements, and compare several variants of ELM algorithms, i.e., the average ELM (AVE-ELM), voting ELM (V-ELM), maximum ELM (MAX-ELM), minimum (MIN-ELM) and the median value filtering ELM (M-ELM). The recognition accuracies in the regular tetrahedron experiments are shown in Table I. In Table I, DTS indicates the regular tetrahedron experiments with different tetrahedron setups. Compared with the regular tetrahedron experiment with a side length of 1 m, the position of the tetrahedron was moved westward by 1 m and moved southward by 1 m. In addition, the tetrahedron was rotated 180 degrees. DGSS indicates regular tetrahedron experiments with different gas source setups. Compared with the regular tetrahedron experiment with a side length of 1 m, the source for the "source in" case was located in the symmetrical position of the original source in Fig. 4 (a) with plane ADE (determined by the points A, D and E) being the symmetry plane, and the distance between the source and the tetrahedron of the "source out" case was doubled (i.e., the distance for this experiment was 1.3 m, compared with 0.65 m for the experiment in Fig. 4 (b)).

TABLE I
RECOGNITION ACCURACY (%) OF THE REGULAR TETRAHEDRON EXPERIMENT USING DIFFERENT ELM-BASED METHODS

Methods	Recognition accuracy (%) with different side length of regular tetrahedron					
	1m	1.5m	2m	DTS[1]	DGSS[2]	Average
ELM-MFC [62]	94.5	93.5	94.0	95.0	85.0	92.4
AVE-ELM	85.7	96.7	98.2	91.4	76.8	89.7
V-ELM	80.0	99.0	100	85.7	84.2	89.8
MAX-ELM	89.2	100	100	92.2	73.0	90.9
MIN-ELM	89.2	100	100	92.3	73.0	90.9
M-ELM	91.3	100	100	97.4	77.6	**93.2**

[1] DTS indicates the regular tetrahedron experiments with different tetrahedron setups.
[2] DGSS indicates regular tetrahedron experiments with different gas source setups.

As can be seen from Table I, based on the raw measured data, the M-ELM method yields the best average recognition accuracy of 93.2%, better than the other ELM-based declaration methods and better than the ELM-MFC.

C. Recognition Accuracy of Irregular Tetrahedron

Table I shows that M-ELM yielded the best average declaration accuracy in the regular tetrahedron experiments. We now ask whether good recognition accuracy can be obtained also in the irregular tetrahedron experiments. Here, based on the regular tetrahedron with a side length of 1 m, two of the four tetrahedral vertices were moved: one was raised by 0.1 m and the other one was lowered by 0.1 m to construct an irregular tetrahedron. The recognition accuracies of the irregular tetrahedron experiments are shown in Table II.

TABLE II
RECOGNITION ACCURACY (%) OF THE IRREGULAR TETRAHEDRON EXPERIMENT USING DIFFERENT ELM-BASED METHODS

Methods	Recognition accuracy (%)
ELM-MFC [62]	93.5
AVE-ELM	88.1
V-ELM	99.3
MAX-ELM	92.3
MIN-ELM	91.2
M-ELM	**100**

As shown in Table II, the raw measured data plus the M-ELM method again achieved the best recognition accuracy of 100% in the irregular tetrahedron experiments, better than the other methods, which further verifies the effectiveness of using the M-ELM method operating on the raw measurements for tetrahedron-based gas source declaration.

VI. CONCLUSION

For gas source declaration, we propose to use a tetrahedral sensor node arrangement (with each sensor node consisting of a gas sensor and an anemometer) and a machine learning approach to distinguish whether the gas source is inside (i.e., the "source in" case) or outside (i.e., the "source out" case) the tetrahedron. We propose the median value filtering based extreme learning machine (M-ELM) source declaration method to declare the "source in" or the "source out" case. We validated the effectiveness of the proposed method for gas source declaration in real-world

experiments, demonstrating in regular and irregular tetrahedron experiments, that the proposed method outperforms the ELM-MFC and other variants of ELM algorithms in terms of gas source declaration accuracy. However, it is worth noting that M-ELM algorithm needs to use multiple ELM algorithms at the same time, and the real-time performance is lower than the classic ELM algorithm. Besides, for the measurement of the same gas concentration, if the ambient temperature and humidity change, the output of the gas sensor may also change. To accurately determine whether the gas source is 'source in' or 'source out', the sensor response signals in various situations need to be trained and learned.

We discuss two ways for constructing the tetrahedral measurement geometry. One is based on a fixed sensor node structure, and the other is based on a mobile sensor node structure. For the mobile sensor node structure, a 3D path planning strategy was proposed and verified through simulations, which provides a valuable guidance for practical applications of the proposed gas source declaration methods.

VI. FUTURE WORK

A. Ways for Tetrahedron Constructing

As illustrated in Section II B, two theoretical ways for tetrahedron construction were described in detail. One of them was verified by experiments and the other by simulation. Both of them use multiple sensor nodes simultaneously. We ask whether it is possible to use only one sensor node. That is the third option: a single mobile sensor that carries out the measurements at the tetrahedron position in sequence, not in parallel. Compared to parallel sensor nodes, a single sensor node has a time delay when traversing four nodes. There is also a delay in the large change of the gas mass. In order to obtain accurate gas information, the sensor node is required to move at a much faster rate than the gas diffusion rate. Therefore, the use of a single sensor node is also a possibility, and we will conduct corresponding research.

B. Irregular Tetrahedron

Table II illustrates that good recognition accuracy of gas source by using an irregular tetrahedron are obtained. While based on the regular tetrahedron whose side length is 1 m, only two sensor nodes were moved by 0.1 m to construct an irregular tetrahedron. Given that different irregular tetrahedron may exist in actual situations, we will continue to study the recognition performance based on other irregular tetrahedrons.

C. Three-class classification

Theoretically, there is a situation where the gas source is placed on the edge/rail of the tetrahedron, but in practice, the more concerned is whether the gas (leak) source is in a certain area. Generally, the position of the four tetrahedron vertices is adjusted dynamically and the gas source is confirmed by the two-class classification method proposed in this paper. We will design a three-class classification algorithm later to verify situation where the gas source is placed on the edge/rail of the tetrahedron through experiments.

REFERENCES

[1] A. P. Ravikumar, J. Wang, A. R. Brandt, "Are optical gas imaging technologies effective for methane leak detection," *Environ. Sci. Technol.*, vol. 51, no. 1, pp. 718–724, Jan. 2017.

[2] A. Nag, A. Zia, X. Li, S. Mukhopadhyay S and J. Kosel, Novel sensing approach for LPG leakage detection: part I: operating mechanism and preliminary results, *IEEE Sens. J.*, vol. 16, no. 4, pp. 996–1003, Feb. 2016.

[3] D. Spirjakin, A. Baranov and S. Akbari, Wearable wireless sensor system with RF remote activation for gas monitoring applications, *IEEE Sens. J.*, vol. 18, no. 7, pp. 2976–2982, Jan. 2018.

[4] L. Marques, U. Nunes and A. T. D. Almeida, Particle swarm-based olfactory guided search, *Auton. Robot.*, vol. 20, no. 3, pp. 277-287, May. 2006.

[5] M. Dunbabin and L. Marques, Robots for environmental monitoring: significant advancements and applications, *IEEE Robot. Autom. Mag.*, vol. 19, no. 1, Mar. 2012.

[6] Y. T. Wei, Q. H. Meng, Y. Q. Jing, Y. J. Liu and M. Zeng, "A portable odor-tracing instrument." *IEEE Trans. Instrum. Meas.*, vol. 65, no. 3, pp. 631–642, 2016.

[7] H. Ishida, Y. Wada, and H. Matsukura, "Chemical sensing in robotic applications: A review," *IEEE Sensors J.*, vol. 12, no. 11, pp. 3163–3173, Nov. 2012.

[8] H. Ishida, K. Suetsugu, T. Nakamoto and T. Moriizumi, "Study of autonomous mobile sensing system for localization of odor source using gas sensors and anemometric sensors," *Sens. Actuators A, Phys.*, vol. 45, no. 2, pp. 153–157, Nov. 1994.

[9] R. A. Russell, D. Thiel, R. Deveza and A. Mackay-Sim, "A robotic system to locate hazardous chemical leaks," in *Proc. IEEE Int. Conf. Robot. Autom.*, 1995, pp. 556–561.

[10] T. R. Consi, J. Atema, C. A. Goudey, J. Cho and C. Chryssostomidis, "AUV guidance with chemical signals," in *Proc. IEEE Symp. Auto. Underwater Veh. Technol.*, 1995, pp. 450–455.

[11] G. Sandini, G. Lucarini and M. Varoli, "Gradient driven self-organizing systems," in *Proc. IEEE/RSJ Int. Conf. Intell. Robots Syst.*, 1993, pp. 429–432.

[12] L. Shu, M. Mukherjee, X. Xu, et al., "A Survey on Gas Leakage Source Detection and Boundary Tracking with Wireless Sensor Networks," *IEEE Access*, vol. 4, pp. 1700–1715, 2016.

[13] F. Lei, L. Yao, D. Zhao, et al., "Energy-Efficient Abnormal Nodes Detection and Handlings in Wireless Sensor Networks," *IEEE Access*, vol. 5, pp. 3393-3409, 2016.

[14] H. Ishida, T. Yamanaka, N. Kushida, T. Nakamoto, and T. Moriizumi, "Study of real-time visualization of gas/odor flow images using gas sensor array," *Sens. Actuator B-Chem*, vol. 65, pp. 14–16, 2000.

[15] A. Lilienthal, F. Streichert and A. Zell, "Model-based shape analysis of gas concentration gridmaps for improved gas source localisation," in *Proc. IEEE Int. Conf. Robotics and Automation* (ICRA), 2005, pp. 3575–3580.

[16] J. Atema, "Eddy chemotaxis and odor landscapes: exploration of nature with animal sensors. *Biol. Bull.*, vol. 191, no. 1, pp. 129–138, 1996.

[17] Schmuker M, Bahr V, Huerta R, "Exploiting plume structure to decode gas source distance using metal-oxide gas sensors," *Sens. Actuator B-Chem.* Vol. 235, pp. 636–646, 2016.

[18] W. Tsujita, A. Yoshino, H. Ishida, T. Moriizumi, "Gas sensor network for air-pollution monitoring," *Sens. Actuator B-Chem.*, vol. 110, no. 2, pp. 304–311, Oct. 2005.

[19] A. Somov, A. Baranov, A. Savkin, D. Spirjakin, A. Spirjakin and R. Passerone, "Development of wireless sensor network for combustible gas monitoring," *Sens. Actuator A-Phys.*, vol. 171, no. 2, pp. 398–405, Nov. 2011.

[20] V. Jelicic, M. Magno, D. Brunelli, G. Paci and L. Benini, "Context-adaptive multimodal wireless sensor network for energy-efficient

gas monitoring," *IEEE Sens. J.*, vol. 13, no. 1, pp. 328–338, Jan. 2013.

[21] T. Zhao and A. Nehorai, "Distributed sequential bayesian estimation of a diffusive source in wireless sensor networks," *IEEE Trans. Signal Process.*, vol. 55, no. 4, pp. 1511–1524, Apr. 2007.

[22] X. H. Kuang and H. H. Shao, "Plume source localization based on Bayes using wireless sensor network," *Acta Armamentarii.*, vol. 29, no. 12, pp. 1474–1478, Dec. 2008.

[23] Q. M. Li, Z. Liu, and X. Xiao, "A gas source localization algorithm based on particle filter in wireless sensor network," International Journal of Distributed Sensor Networks., vol. 1, pp. 2514–2518, 2015

[24] L. Shu, M. Mukherjee, X. L. Xu, K. Wang and X. L. Wu, "A survey on gas leakage source detection and boundary tracking with wireless sensor networks," *IEEE Access.*, vol. 4, pp. 1700–1715, Apr. 2016.

[25] S. Y. Li, J. J. Zhang, D. Yan, et al., "Leak detection and location in gas pipelines by extraction of cross spectrum of single non-dispersive guided wave modes," *J. Loss Prev. Process Ind*., vol. 44, pp. 255–262, Nov. 2016.

[26] X. Bian, Y. Zhang, Y. B. Li and X. Y. Gong, "A new method of using sensor arrays for gas leakage location based on correlation of the time-space domain of continuous ultrasound," *Sensors*, vol. 15, no. 4, pp. 8266–8283, Apr. 2015.

[27] D.L Ma, Wei T., Q. S. Wang, et al., "Location of contaminant emission source in atmosphere based on optimal correlated matching of concentration distribution," *Process Saf. Environ. Protect*., vol. 117, pp. 498–510, Jul. 2018.

[28] B. Luo, Q. H. Meng, J. Y. Wang and S. G. Ma, "Simulate the aerodynamic olfactory effects of gas-sensitive UAVs: A numerical model and its parallel implementation," *Adv. Eng. Softw*., vol. 102, pp. 123–133, Dec. 2016.

[29] A. T. Hayes, A. Martinoli, R. M. Goodman, "Distributed odor source localization," *IEEE Sens. J*., vol. 2, no. 3, pp. 260–271, Jun, 2002.

[30] H. Ishida, H. Tanaka, H. Taniguchi and T. Moriizumi, "Mobile robot navigation using vision and olfaction to search for a gas/odor source," *Auton. Robot*, vol. 20, pp. 231–238, 2006.

[31] G. Kowadlo, D. Rawlinson, R. A. Russell, R. Jarvis, "Bi-modal search using complementary sensing (olfaction/vision) for odour source localisation," in *Proc. IEEE ICRA*, 2006, pp. 2041–2046.

[32] D. Martinez, L. Perrinet, "Cooperation Between Vision and Olfaction in a Koala Robot," In *Report on the Workshop on Neuromorphic Engineering*, 2002, pp. 51–53.

[33] A. Lilienthal, H. Ulmer, H. Fröhlich, A. Stützle, F. Werner and A. Zell, "Gas Source Declaration with a Mobile Robot," *Proceedings of the IEEE International Conference on Robotics and Automation* (ICRA), 2004, pp. 1430–1435.

[34] A. Lilienthal, A. Loutfi and T. Duckett, "Airborne Chemical Sensing with Mobile Robots," *Sensors*, vol. 6, pp. 1616–1678, 2006.

[35] R. A. Russell, A. Bab-Hadiashar, R. L. Shepherd, and G. G. Wallace, "A comparison of reactive chemotaxis algorithms," *Robot. Auton. Syst*., vol. 45, pp. 83 – 97, 2003.

[36] A. Lilienthal and T. Duckett, "Experimental analysis of smelling braitenberg vehicles," *Proceedings of the IEEE International Conference on Advanced Robotics* (ICAR 2003), Coimbra, Portugal, 2003, pp. 375–380.

[37] M. Vuka, F. Amigoni, M. Schmuker, E. Schaffernicht, V. H. Bennetts, A. J. Lilienthal, "Exploration and localization of a gas source with MOX gas sensors on a mobile robot - a gaussian regression bout amplitude approach," *International Symposium on Olfaction and Electronic Nose* (ISOEN), 2017, pp. 1–3.

[38] Z. Pasternak, F. Bartumeus, F. W. Grasso, "Levy-taxis: a novel search strategy for finding odor plumes in turbulent flow-dominated environments," *J. Phys. A-Math. Theor*., vol. 42, no. 43, 434010, Otc. 2009.

[39] S. Shigaki, T. Sakurai, N. Ando, D. Kurabayashi and R. Kanzaki, "Time-varying moth-inspired algorithm for chemical plume tracing in turbulent environment," *IEEE Robotics & Automation Letters*," vol. 3, no. 1, pp. 76–83, Jan. 2018.

[40] J. G. Li, Q. H. Meng, Y. Wang and M. Zeng, "Odor source localization using a mobile robot in outdoor airflow environments with a particle filter algorithm," *Auton. Robot.*, vol. 30, no. 3, pp. 281–292, Apr. 2011.

[41] H. Li, Y. Yang, X. Qiu, et al., "Gravitation-Based 3D Redeployment Schemes for the Mobile Sensors and Sink in Gas Leakage Monitoring," *IEEE Access*, vol. 5, pp. 8545–8558, 2017.

[42] J. Huseynov, S. Baliga, M. Dillencourt, et al., "Gas-leak localization using distributed ultrasonic sensors," *Proceedings of SPIE - The International Society for Optical Engineering*., 2009, 7293.

[43] K. A. Gillis, M. R. Moldover and J. B. Mehl, "Detecting leaks in gas-filled pressure vessels using acoustic resonances," *Rev. Sci. Instrum*., vol. 87, no.5, 054901, May. 2016.

[44] S. Y. Li, Y. M. Wen, P. Li and J. Yang, "Determination of acoustic speed for improving leak detection and location in gas pipelines," *Rev. Sci. Instrum*., vol. 85, no. 2, 024901, Feb. 2014.

[45] H. Ishida, M. Zhu, K. Johansson and T. Moriizumi, "Three-dimensional gas/odor plume tracking with blimp," in *Proc. Asia–Pacific Conf. Transducers Micro-Nano Technol.* Sapporo., 2004, pp. 117–120.

[46] Y. Kuroki, G. S. Young, S. E. Haupt, "UAV navigation by an expert system for contaminant mapping with a genetic algorithm," *Expert Syst. Appl.*, vol. 37, no. 6, pp. 4687–4697, Jun. 2010.

[47] P. P. Neumann, S. Asadi, A. J. Lilienthal, M. Bartholmai and J. H. Schiller, "Autonomous gas-sensitive microdrone: wind vector estimation and gas distribution mapping," *IEEE Robot. Autom. Mag.*, vol. 19, no. 1, pp. 50–61, Mar. 2012.

[48] P. P. Neumann, V. H. Bennetts, A. J. Lilienthal and M. Bartholmai, "Gas source localization with a micro-drone using bioinspired and particle filter-based algorithms," *Adv. Robot.*, vol. 27, no. 9, pp. 725–738, Jun. 2013.

[49] B. Luo, Q. H. Meng, J. Y. Wang and M. Zeng, "A flying odor compass to autonomously locate the gas source," *IEEE Trans. Instrum. Meas.*, vol. 67, no. 1, pp. 137–149, Jan. 2018.

[50] A. D. C. Albornoz, A. B. Rodríguez, A. R. G. Ramirez, et al., "An approach for robot-based odor navigation," *J. Med. Biol. Eng.*, vol. 32, no. 6, pp. 453–456, 2012.

[51] M. Dani, P. Tomàs, J. Moreno and M. Tresanchez, "A mobile robot agent for gas leak source detection," *Advances in Intelligent Systems and Computing*., vol. 293, pp. 19–25, Jan. 2014.

[52] M. Vuka, E. Schaffernicht, M. Schmuker, et al., "Exploration and localization of a gas source with MOX gas sensors on a mobile robot-A Gaussian regression bout amplitude approach," *ISOCS/IEEE International Symposium on Olfaction and Electronic Nose* (ISOEN)., 2017.

[53] G. B. Huang, L. Chen, "Convex incremental extreme learning machine," *Neurocomputing*, vol. 70, no. 16–18, pp. 3056–3062, Oct. 2007.

[54] N. Y. Liang, G. B. Huang, P. Saratchandran, N. Sundararajan, "A fast and accurate online sequential learning algorithm for feedforward networks," *IEEE Trans. Neural Netw. Learn. Syst*., vol. 17, no. 6, pp. 1411–1423, Nov. 2006.

[55] H. J. Rong, G. B. Huang, N. Sundararajan, P. Saratchandran, "Online sequential fuzzy extreme learning machine for function approximation and classification problems," *IEEE Trans. Syst.,Man, Cybern. B, Cybern*., vol. 39, no. 4, pp. 1067–1072, Aug. 2009.

[56] G. Huang, S. J. Song, J. N. D. Gupta, C. Wu, "Semi-supervised and unsupervised extreme learning machines," *IEEE T. Cybern.*, vol. 44, no. 12, pp. 2405–2417, Dec. 2014.

[57] L. L. C. Kasun, H. Zhou, G. B. Huang, C. M. Vong "Representational Learning with Extreme Learning Machine for Big Data," *IEEE Intel. Syst*., vol. 28, no. 6, pp. 31–34, 2013.

[58] Y. M. Yang, Y. N. Wang, X. F. Yuan, "Bidirectional Extreme Learning Machine for Regression Problem and Its Learning Effectiveness," *IEEE Trans. Neural Netw. Learn. Syst.*, vol. 23, no. 9, pp. 1498–1505, Sept. 2012.

[59] W. P. Cao, Z. Ming, X. Z. Wang, S. B. Cai, "Improved bidirectional extreme learning machine based on enhanced random search. Memetic Computing," *Memet. Comput*., vol. 11, no. 1, pp. 19–26, Mar. 2019.

[60] W. P. Cao, X. Z. Wang, Z. Ming, J. Z. Gao, "A review on neural networks with random weights," *Neurocomputing*, vol. 275, no. 31, pp. 278–287, Jan. 2019.

[61] L. J. Duan, H. Y. Zhong, J. Miao and Z. Yang, "A voting optimized strategy based on ELM for improving classification of motor

imagery BCI data," *Cogn. Comput..*, vol. 6, no. 3, pp. 477–483, Sep. 2014.

[62] H. R. Hou, Y. Tong, C. Ren and Q. H. Meng, "A gas source declaration scheme based on a tetrahedral sensor structure in three-dimensional airflow environments," *Rev. Sci. Instrum.*, vol. 90, no. 2, 024104, Feb. 2019.

[63] G. B. Huang, "Learning capability and storage capacity of two-hidden-layer feedforward networks," *IEEE Trans. Neural Netw. Learn. Syst..*, vol. 14, no. 2, pp. 274–281, Mar. 2003.

[64] G. B. Huang and H. A. Babri, "Upper bounds on the number of hidden neurons in feedforward networks with arbitrary bounded nonlinear activation functions," *IEEE Trans. Neural Netw. Learn. Syst*., vol. 9, no. 1, pp. 224–229 Feb. 1998.

[65] G. B. Huang, H. Zhou, X. Ding and R. Zhang, "Extreme learning machine for regression and multiclass classification," *IEEE Trans. Syst.,Man, Cybern. B, Cybern*., vol. 42, no. 2, pp. 513–529, Oct. 2011.